

Transition to Turbulence and Mixing in a Viscoelastic Fluid Flowing Inside a Channel with a Periodic Array of Cylindrical Obstacles

Muzio Grilli, Adolfo Vázquez-Quesada, and Marco Ellero

Institute of Aerodynamics and Fluid Mechanics, Technische Universität München, 85747 Garching, Germany

(Received 6 May 2012; revised manuscript received 9 October 2012; published 22 April 2013)

Using Lagrangian simulations of a viscoelastic fluid modeled with an Oldroyd-B constitutive equation, we demonstrate that the flow through a closely spaced linear array of cylinders confined in a channel undergoes a transition to a purely elastic turbulent regime above a critical Weissenberg number (We). The high- We regime is characterized by an unsteady motion and a sudden increase in the flow resistance in qualitative agreement with experimental observations. Furthermore, a power-law scaling behavior of the integral quantities as well as enhanced mixing of mass is observed. A stability analysis based on the dynamic mode decomposition method allows us to identify the most energetic modes responsible for the unsteady behavior, which correspond to filamental structures of polymer over- or underextension advected by the main flow preserving their shape. These time-dependent flow features strictly resemble the elastic waves reported in recent numerical simulations.

DOI: [10.1103/PhysRevLett.110.174501](https://doi.org/10.1103/PhysRevLett.110.174501)

PACS numbers: 47.15.G-, 47.50.Gj, 47.56.+r

Elastic turbulence represents an intriguing phenomenon occurring in complex flows of polymer solutions and corresponding to the onset of a randomly fluctuating fluid motion even in the creeping flow limit, at vanishing Reynolds number. Although the study of elastic instabilities in complex fluids dates back to the early 1990s [1,2], it was not until the seminal paper of Steinberg and Groisman [3] that a complex global flow motion was experimentally observed and the term “elastic turbulence” was coined. Although there is no common agreement on the definition of “turbulence,” the term was introduced in Ref. [4] due to the identification of strong similarities in the phenomenology observed in the flow of polymer suspensions with those commonly characterizing ordinary hydrodynamic turbulence: namely, (i) significant increase in flow resistance, (ii) randomly fluctuating fluid motion with fluctuations increasing with the liquid elasticity, (iii) broad continuum range of temporal or spatial frequencies involved, with power-law spectral scaling behavior, (iv) enhanced mixing of mass. On the basis of these analogies, the work of Ref. [4] shows that elasticity-induced turbulence could be obtained through a moderate increase in the We number. In such conditions, the flow is characterized by features that are comparable to those observed in hydrodynamic turbulence for Re numbers of around 10^4 .

In this Letter, we report evidence of purely elastic instability and transition to turbulence and mixing in a wall-bounded periodic flow geometry characterized by a linear array of cylinders confined in a channel. This flow geometry and the corresponding unbounded one (square array of cylinders) have been widely investigated in the past, both experimentally and numerically, with controversial results. In particular, the unbounded case has been investigated experimentally in Refs. [5–8], where elastic instabilities

were generally observed to show up together with a modification of the global flow behavior: as a critical Weissenberg number is achieved, flow quantities start to exhibit fluctuations that increase in magnitude as the effect of liquid elasticity becomes more pronounced. Moreover, this phenomenon is accompanied by an abrupt increase in the flow resistance, which is believed to be related to a nonlinear transition from a steady state towards a more dissipative time-dependent flow structure [7]. Less effort has been devoted in the past to the experimental study of the corresponding wall-bounded geometry; nevertheless, analogous flow features have been reported in the literature [8,9]. Although the wall-bounded two-dimensional flow was experimentally [9] and numerically [10] found to be unstable to three-dimensional perturbations at a given critical Weissenberg number, to date no numerical method has been able to predict either the unsteady behavior or the large abrupt drag increase observed in experiments. In Ref. [11], two-dimensional Lagrangian simulations using a particle method [smoothed particle hydrodynamics (SPH)] allowed us to observe the transition mentioned above at a critical Weissenberg number of $O(1)$, significantly smaller than the one considered to be the threshold for the onset of three-dimensional flow (~ 1.55). In this Letter, we perform a detailed investigation of the flow transition process using the dynamic mode decomposition (DMD) approach recently developed in Ref. [12]. DMD is a technique that allows for a modal analysis of a data sequence, without resorting to a numerical solver or an underlying model [12]. In the case of a linearized flow (i.e., a flow of small perturbation about a steady base flow), the extracted structures are equivalent to global eigenmodes. For a nonlinear flow, the decomposition produces modes that express the dominant dynamic behavior captured in the data sequence. Such analysis enables us to extract

dynamic neutrally stable coherent structures from numerical snapshots of flow fields. The main aim of this investigation is to prove that this transition leads eventually to a flow regime that exhibits several features of the so-called elastic turbulence.

The problem considered in this work is sketched in Fig. 1 and can be formulated as follows: a cylinder of radius $R_c = 1$ is placed on the centerline of a two-dimensional channel characterized by a half-height $H_c = 2$. The liquid in between is driven by a constant body force. No-slip velocity boundary conditions are applied to the solid channel walls and on the cylinder surface, while periodic boundary conditions are considered along the streamwise direction, producing a linear array structure of spatial period $L_c = 2.5$. As a viscoelastic constitutive equation, we adopt the Oldroyd-B model, which is considered to match fairly well the main properties of Boger liquids commonly used experimentally [13]. Such a model has been also adopted in recent numerical simulations of elastic instabilities [14–17]. Coupled to the momentum conservation, it produces the following set of equations written in a Lagrangian framework,

$$\begin{aligned} \frac{d\mathbf{v}}{dt} &= -\frac{\nabla p}{\rho} + \frac{\eta_s}{\rho} \Delta \mathbf{v} + \frac{1}{\rho} \nabla \cdot \boldsymbol{\tau} \\ \frac{d\mathbf{c}}{dt} &= \boldsymbol{\kappa} \cdot \mathbf{c} + \mathbf{c} \cdot \boldsymbol{\kappa}^T + \frac{1}{\lambda} [\mathbf{1} - \mathbf{c}], \end{aligned} \quad (1)$$

where $\boldsymbol{\tau} = G(\mathbf{c} - \mathbf{1})$ is the polymeric stress tensor, $G = \eta_p/\lambda$ is the shear modulus, λ is the elastic relaxation time, \mathbf{c} is the dimensionless conformation tensor describing the average alignment or stretching of polymer molecules, and $\boldsymbol{\kappa} = (\nabla \mathbf{v})^T$ is the velocity gradient tensor. To rule out the effect of inertia, a Reynolds number $\text{Re} = R_c \langle v \rangle \rho / \eta = 2.4 \times 10^{-2}$ is used, where the total viscosity η contains two contributions: the dynamic solvent viscosity $\eta_s = 24.58$ and the polymeric viscosity $\eta_p = 17.08$. This gives a factor $\beta = \eta_s/\eta = 0.59$ commonly chosen in benchmarks for the Oldroyd-B fluid. The Weissenberg number is defined as $We = \lambda \langle v \rangle / R$. In this work, simulations with $We \in [0; 1.6]$ are performed. At greater We values, the flow has shown to develop a weak component in the neutral cylinder-axis direction [10]. For this reason, results of two-dimensional simulations are unable to capture the correct physics in such flow conditions. The previous

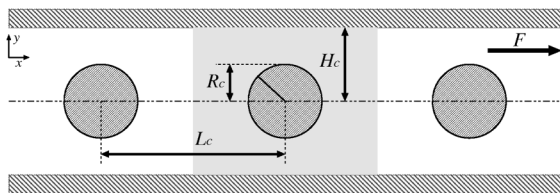


FIG. 1. Schematic representation of the confined-cylinder flow geometry.

equations are discretized in a Lagrangian framework by using the SPH method [18] by considering a minimum particle spacing $\Delta x = 0.02R_c$, as discussed in detail in Ref. [11].

Abrupt drag increase.—One of the main features characterizing a transition to a turbulent state is represented by a sudden increase in the flow resistance. In the case of a viscoelastic flow through a cylinder array, the onset of transition can be estimated by the enhancement factor defined as the viscoelastic drag acting on the cylinder normalized by the drag in the laminar Newtonian case [$F_D(We)/F_D^{\text{Newt}}$]. Figure 2 shows the enhancement factor as a function of We . Slight deviations from unity up to $We = We_c \approx 1$ are observed, indicating that the viscoelastic solution is close to the base Newtonian one. For $We \geq We_c$, our numerical results exhibit an abrupt drag increase (approximately 100% for $We \sim 1.6$) in qualitative agreement with observations made in experimental studies of both confined and unconfined array of cylinders [5,7–9]. Numerical convergence of the results was proven in Ref. [11]. The sudden increase in the flow resistance starting at $We_c \approx 1$ corresponds to inception of an elastic instability, namely, the flow becomes two-dimensionally unsteady with fluctuations increasing with We . Figure 2 also shows the rms of the time-dependent lift acting on the cylinder for different We values. Amplitudes increase with We suggesting increasingly unsteady behavior. It should be noted that this sudden increase in the drag and the corresponding unsteady flow behavior have never been reported numerically. Indeed, previous numerical calculations of the linearized Oldroyd-B equations for this specific problem predicted absolute global stability of the steady base solution at every We in contrast to experimental observations [9]. It should be underlined that a condition of linear stability does not prevent the flow from becoming nonlinearly unstable [19,20] upon proper choice of a finite amplitude perturbation.

Elastic instability: unsteady behavior.—To understand the main mechanism of the change of flow configuration

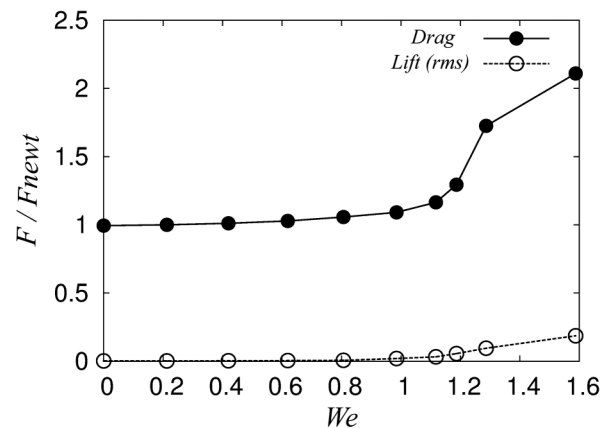


FIG. 2. Drag force and rms of the lift acting on the cylinder as a function of the Weissenberg number.

towards unsteady behavior, we consider next a DMD analysis recently developed in Ref. [12]. To this aim, velocity or stress fields defined on Lagrangian particle trajectories are interpolated at constant time steps on a fixed grid once the stationary unsteady state is achieved and the standard DMD procedure is applied. Figure 3 shows the relative amplitude of the dynamic modes in the temporal frequency domain $\omega = 1/T$ for $We = 0.4$ and $We = 1.3 \geq We_c$. In the former case, a flattened spectrum is observed, suggesting that no coherent structures are visible within the threshold fluctuation level of SPH. At $We = 1.3$, a main peak is produced corresponding to a dominant neutrally stable mode of frequency $\omega = \bar{\omega} \approx 0.4$ close to the characteristic elastic frequency $\omega_e = 1/\lambda = 0.5$. Interestingly, an increased DMD amplitude is obtained with decreasing ω_e approaching the flow frequency $\omega_{fl} = \langle v \rangle / L_c = 0.25$. Such a finding suggests the possible existence of a resonant mechanism in which the main liquid elastic mode interacts with the periodic modulation of the geometry. A similar interaction mechanism of resonance between flow and an elastic filament has been proposed in Ref. [21] in the framework of the laminar Newtonian flow over a cylinder. Note that simulations obtained using different particle resolutions ($P1$, $P2$, $P3$) deliver the same results for the main frequency characterizing the dominant mode of the instability, which excludes the existence of a spurious, resolution-dependent behavior. At larger frequencies, amplitudes do not drop suddenly to zero, but they undergo a continuous decay. Figure 4 shows different snapshots of the polymer elongation $\text{Tr}(\mathbf{c})$ for $We = 1.3$ after transition, corresponding to the most energetic unsteady mode $\bar{\omega}$. The velocity field corresponding to this mode is smooth in space and weakly oscillating in time in a way that its changes are difficult to visualize on single snapshots and can be better appreciated in the videos provided within the Supplemental Material [22]. Note the oscillatory motion undergone by the streamlines in the

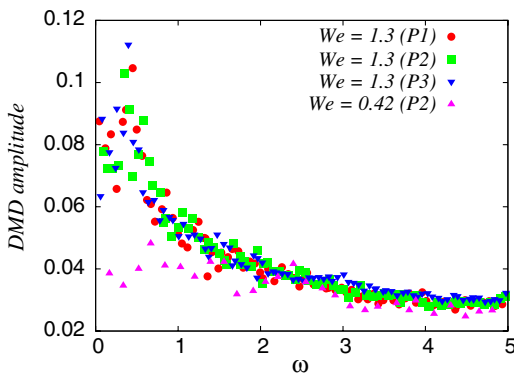


FIG. 3 (color online). Amplitudes of the dynamic modes vs frequency $\omega = 1/T$ for two typical Weissenberg numbers below and above instability inception. Numerical resolutions $P1$, $P2$, $P3$ used here correspond to a number of particles in the cross-stream directions $N_y = 120, 144, 192$ and show convergence in the DMD spectra.

recirculating region within the cylinder gap that produces a cross-stream time-dependent flow of mass breaking the plane symmetry. In contrast to the velocity field, the polymer elongation field shows a very complex behavior characterized by red areas (indicated by the label 1) of relative overextension (with respect to the steady base solution) and blue areas (indicated by the label 2) of local polymer contraction. Moreover, a marked unsteady behavior is visible, especially near the wall where structures are advected by the local flow field, almost preserving their shape. These inhomogeneities are absent at $We = 0.4$ where no coherent unsteady behavior emerges (see Fig. 3). These structures featured by the polymer elongation field resemble the nonstationary states predicted theoretically in Ref. [23] and recently observed and described in Refs. [17,24] corresponding to a traveling elastic waves regime. The wavy elastic motion and its coupling with the underlying velocity field is the main driver responsible for the onset of temporal dependencies in the integral quantities and can favor the eventual mixing of mass and momentum.

Power spectrum.—We analyze in detail the consequence of these unsteady structures on the fluctuating dynamics. A characteristic feature of elastic turbulence is represented by the excitation of the fluid motion over a broad continuum range of frequencies. Figure 5 shows the power spectral densities of the velocity fluctuations in different locations within the flow domain. For $We = 1.3 > We_c$, a power-law decay $\omega^{-\alpha}$ is observed over approximately 1 decade in the frequency. The observed power-law exponent α features a value higher than 3, significantly greater than the Kolmogorov exponent ($\alpha_K = 5/3$), in agreement with theoretical predictions [23], experimental results [4], and previous numerical simulations [16].

It has also to be noted that the intensities of the fluctuations in the two stagnation points within the intercylinder gap (points 4 and 5) are significantly smaller than those in the remaining locations. This is consistent with the fact that the above mentioned positions are characterized by an average streamwise velocity approaching zero, whereas that is not the case for the remaining locations. Furthermore, stronger fluctuations arise in the near-wall regions (points 1 and 3) rather than in the bulk (point 2). We believe such increased level of velocity fluctuation to

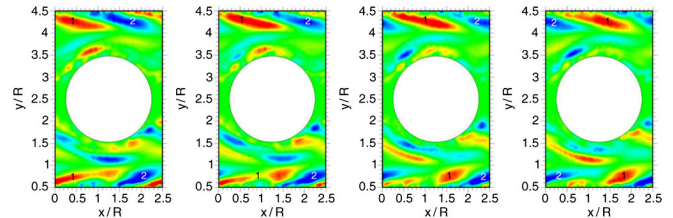


FIG. 4 (color online). Snapshot of the polymer elongation $\text{Tr}(\mathbf{c})$ corresponding to the dominant mode of frequency $\omega = \bar{\omega} \approx 0.4$ for $We = 1.3$ at different times after transition.

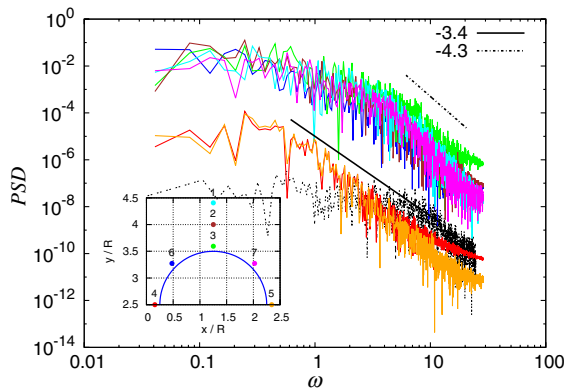


FIG. 5 (color online). Power spectral density of the velocity signal in several locations for the $We = 1.3$ case. The location of the probes is indicated in the inset. The PSD spectrum obtained in the position 2 for the Newtonian case is indicated by dotted dashed lines.

be directly related to the presence of the strong near-wall stress inhomogeneities shown in Fig. 4. Note also from Fig. 5 that, although similar, the power-law exponent α in the stagnation points is slightly smaller than that in the bulk flow. These two points are located within the low-velocity separated region and are not directly affected by the coherent structures discussed above. We believe that the persistence of a power-law behavior (although with smaller intensity) in the stagnation region is the result of a fluctuating velocity field in the gap being purely *induced* by the chaotic flow motion occurring *outside* the separation region. The different driving mechanisms of the two processes could explain the change in the exponent α ($\alpha \approx 4.3 \rightarrow 3.4$) observed here.

Mixing.—As a final proof, we present a study of the effect of the elastic transition discussed above on the dispersion of passive tracers. The Lagrangian character of SPH allows us to follow directly fluid trajectories without the need of extra tracking particles. At time $t = 0$, we mark in black all the fluid particles lying on a layer of thickness $0.2R_c$ adjacent to the upper wall and monitor their evolution for different We numbers. Figure 6 shows the space-time diagrams obtained by plotting continuously temporal snapshots of the brightness profiles taken along a single perpendicular line between the cylinder and channel wall. The upper figure ($We = 0.4$) shows that, although there is a small isotropic numerical dispersion, no anisotropic mixing takes place. Instead, at $We = 1.3$, chaotic structures corresponding to large irregular oscillations in the profile of the (black) dye in the (white) bulk fluid occur. Expulsion of (black) material away from the wall is balanced by injection of (white) bulk fluid within the near-wall region. Such a phenomenon increases with time and eventually leads to a much thicker mixed layer than in the previous case. At time $t = 12$, for $We = 0.4$, the layer thickness saturates to a value very close to the initial one $h \approx 0.2R_c$, whereas for $We = 1.3$ at the same flow time we

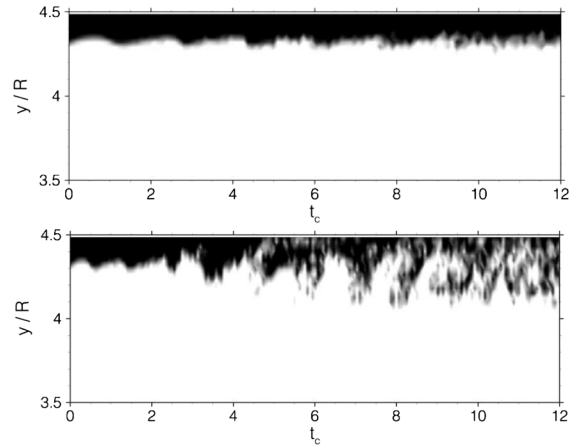


FIG. 6. Space-time diagrams for the evolution of mixing layers of a black dye initially placed near the wall, for $We = 0.4, 1.3$.

have $h \approx 0.5R_c$. The evolution of the mixing layers in the two cases can be also appreciated in the Supplemental Material [22].

Conclusions.—In this Letter, we have demonstrated for the first time that an elastic turbulent regime can be reproduced numerically in the flow of an Oldroyd-B liquid in a complex periodic channel flow geometry. In order to support this claim, three main characteristic features of the turbulent behavior have been analyzed and reported, namely, the abrupt increase of the flow resistance, a broad range of spatial or temporal scales present in the fluid motion, and enhanced mixing of mass. The chaotic motion is triggered by an initial steady-unsteady transition in the solution at $We \sim O(1)$ for which a dominant unsteady neutrally stable mode exists. This slowly fluctuating mode drains energy from the base steady solution, reducing its total kinetic energy and feeding it into complex polymer dynamics, characterized by the unsteady motion of areas undergoing polymer over- or underextension. At sufficiently great Weissenberg numbers, the mode is able to mediate the energy transfer towards smaller scales producing increasingly irregular flow patterns and enhanced mixing. The latter feature could be of paramount importance in microfluidics conditions where mixing is generally limited by the molecular diffusion [25–27]. It has been noted that the introduction of finite polymer extensibility can have a stabilizing effect on the dynamics [28,29]. We have explicitly checked that the use of a FENE-CR model does not alter the results shown here, provided that realistically large values of the polymer extensibility are considered [30].

The authors would like to thank R. I. Tanner, F. T. Pinho, and specially the Reviewers for valuable discussions. Financial support was provided by the DFG via Grant No. EL 503/1-1. The first author (M. G.) also gratefully acknowledges the support of the TUM Graduate School Faculty Graduate Center for Mechanical Engineering. Computer resources for this project were provided by the Leibniz Supercomputing Centre under Grant No. pr58ye.

- [1] R. G. Larson, E. S. G. Shaqfeh, and S. J. Muller, *J. Fluid Mech.* **218**, 573 (1990).
- [2] E. S. G. Shaqfeh, *Annu. Rev. Fluid Mech.* **28**, 129 (1996).
- [3] A. Groisman and V. Steinberg, *Nature (London)* **405**, 53 (2000).
- [4] A. Groisman and V. Steinberg, *New J. Phys.* **6**, 29 (2004).
- [5] L. Skartsis, B. Khomami, and J. L. Kardos, *J. Rheol.* **36**, 589 (1992).
- [6] C. Chmielewski and K. Jayaraman, *J. Non-Newtonian Fluid Mech.* **48**, 285 (1993).
- [7] B. Khomami and L. D. Moreno, *Rheol. Acta* **36**, 367 (1997).
- [8] K. Arora, R. Sureshkumar, and B. Khomami, *J. Non-Newtonian Fluid Mech.* **108**, 209 (2002).
- [9] A. W. Liu, Ph.D. dissertation, Massachusetts Institute of Technology, Cambridge, MA (1997).
- [10] M. D. Smith, Y. L. Joo, R. C. Armstrong, R. A. Brown, and R. Sureshkumar, *J. Non-Newtonian Fluid Mech.* **109**, 13 (2003).
- [11] A. Vázquez-Quesada and M. Ellero, *J. Non-Newtonian Fluid Mech.* **167–168**, 1 (2012).
- [12] P. J. Schmid, *J. Fluid Mech.* **656**, 5 (2010).
- [13] D. F. James, *Annu. Rev. Fluid Mech.* **41**, 129 (2009).
- [14] R. J. Poole, M. A. Alves, and P. J. Oliveira, *Phys. Rev. Lett.* **99**, 164503 (2007).
- [15] B. Thomases and M. Shelley, *Phys. Rev. Lett.* **103**, 094501 (2009).
- [16] S. Berti, A. Bistagnino, G. Boffetta, A. Celani, and S. Musacchio, *Phys. Rev. E* **77**, 055306(R) (2008).
- [17] S. Berti and G. Boffetta, *Phys. Rev. E* **82**, 036314 (2010).
- [18] A. Vázquez-Quesada, M. Ellero, and P. Español, *Phys. Rev. E* **79**, 056707 (2009).
- [19] B. Meulenbroek, C. Storm, V. Bertola, C. Wagner, D. Bonn, and W. van Saarloos, *Phys. Rev. Lett.* **90**, 024502 (2003).
- [20] A. N. Morozov and W. van Saarloos, *Phys. Rev. Lett.* **95**, 024501 (2005).
- [21] S. Bagheri, A. Mazzino, and A. Bottaro, *Phys. Rev. Lett.* **109**, 154502 (2012).
- [22] See Supplemental Material at <http://link.aps.org/supplemental/10.1103/PhysRevLett.110.174501> for reconstruction of the flow fields from the dominant mode at $\omega = 0.4$.
- [23] A. Fouxon and V. Lebedev, *Phys. Fluids* **15**, 2060 (2003).
- [24] D. G. Thomas, B. Khomami, and R. Sureshkumar, *J. Fluid Mech.* **620**, 353 (2009).
- [25] A. Groisman and V. Steinberg, *Nature (London)* **410**, 905 (2001).
- [26] J. A. Pathak, D. Ross, and K. B. Migler, *Phys. Fluids* **16**, 4028 (2004).
- [27] H. Y. Gan, Y. C. Lam, N. T. Nguyen, K. C. Tam, and C. Yang, *Microfluid. Nanofluid.* **3**, 101 (2006).
- [28] B. Sadanandan and R. Sureshkumar, *J. Non-Newtonian Fluid Mech.* **122**, 55 (2004).
- [29] B. Sadanandan and R. Sureshkumar, *J. Non-Newtonian Fluid Mech.* **140**, 108 (2006).
- [30] R. Sizaire and V. Legat, *J. Non-Newtonian Fluid Mech.* **71**, 89 (1997).